

# PROCEEDINGS OF SPIE

[SPIDigitalLibrary.org/conference-proceedings-of-spie](https://spiedigitallibrary.org/conference-proceedings-of-spie)

## Slepian guided filtering of graph signals

Miljan Petrović, Dimitri Van De Ville

Miljan Petrović, Dimitri Van De Ville, "Slepian guided filtering of graph signals," Proc. SPIE 11138, Wavelets and Sparsity XVIII, 111380D (9 September 2019); doi: 10.1117/12.2528827

**SPIE.**

Event: SPIE Optical Engineering + Applications, 2019, San Diego, California, United States

# Slepian Guided Filtering of Graph Signals

Miljan Petrović<sup>a,b</sup> and Dimitri Van De Ville<sup>a,b</sup>

<sup>a</sup>Institute of Bioengineering, École Polytechnique Fédérale de Lausanne, Campus Biotech, Geneva, Switzerland

<sup>b</sup>Department of Radiology and Medical Informatics, University of Geneva, Geneva, Switzerland

## ABSTRACT

Joint localization of graph signals in vertex and spectral domain is achieved in Slepian vectors calculated by either maximizing energy concentration ( $\mu$ ) or minimizing modified embedded distance ( $\xi$ ) in the subgraph of interest. On the other hand, graph Laplacian is extensively used in graph signal processing as it defines graph Fourier transform (GFT) and operators such as filtering, wavelets, etc. In the context of modeling human brain as a graph, low pass (smooth over neighboring nodes) filtered graph signals represent a valuable source of information known as aligned signals. Here, we propose to define GFT and graph filtering using Slepian orthogonal basis. We explored power spectrum density estimates of random signals on Erdős–Rényi graphs and determined local discrepancies in signal behavior which cannot be accessed by the graph Laplacian, but are detected by the Slepian basis. This motivated the application of Slepian guided graph signal filtering in neuroimaging. We built a graph from diffusion-weighted brain imaging data and used blood-oxygenation-level-dependent (BOLD) time series as graph signals residing on its nodes. The dataset included recordings of 21 subjects performing a working memory task. In certain brain regions known to exhibit activity negatively correlated to performing the task, the only method capable of identifying this type of behavior in the bandlimited framework was  $\xi$ -Slepian guided filtering. The localization property of the proposed approach provides significant contribution to the strength of the graph spectral analysis, as it allows inclusion of a priori knowledge of the explored graph's mesoscale structure.

**Keywords:** Slepian, graph, filtering, neuroscience, brain, spectrum

## 1. INTRODUCTION

Complex systems and dynamic processes existing on top of them are successfully modeled as graphs with nodes connected by edges reflecting the intrinsic relationships between them, and signals whose samples are associated with the graph nodes. This framework referred to as graph signal processing (GSP) has brought insight in many different scientific disciplines<sup>1</sup> including image processing, neuroscience, geoscience, etc. The key concepts of the framework are generalizations of the Fourier transform, filtering, convolution, wavelets, and other operators, from 1-dimensional to the domain of graph vertices.<sup>2–4</sup> Strength of this methodology is the ability to process signals with respect to the underlying pattern of connectivity between signal origins.

On the other hand, the question of what would be the graph signal mostly concentrated in a certain subset of nodes has been addressed by graph Slepian vectors<sup>5,6</sup> deriving from a more general continuous framework.<sup>7</sup> Slepian functions allowed for an appropriate signal sampling and reconstruction<sup>8</sup> as well as sophisticated graph embedding solutions.<sup>9</sup>

Whereas GSP focuses on processing signals living on the graph, Slepian analysis explores the properties of the graph itself. The idea of merging the two methodologies seems beneficial as it would provide a framework for processing signals on the nodes while taking into account the *mesoscale local* features of the underlying graph besides the immediate neighborhood node connectivity. Here, we investigate one possible ingredient of such a framework and we will refer to it as Slepian guided filtering of graph signals. However, this kind of framework comes with certain precautions regarding theoretical conditions for a valid spectral graph analysis. Furthermore, depending on the explored graph, one may indeed benefit from including Slepian vectors into the

---

Further author information: (Send correspondence to M.P.)

M.P.: E-mail: miljan.petrovic@epfl.ch

filtering procedure, but this is for sure not guaranteed as the graph itself may not exhibit a modular structure.<sup>10</sup> Hence, we devoted the work presented in this paper to explore the benefits of Slepian guided filtering in the context of random graphs and human brain models, while considering the theoretical circumstances of such a procedure.

In the next sections of the paper we briefly recall the mathematical basis of GSP (Sec. 2.1) and graph Slepian (Sec. 2.2), and build upon this to present Slepian guided filtering (Sec. 3). Then, we demonstrate the results of a power spectrum analysis of random signals on graphs with random connectivity, in order to provide motivation for an application to real-world data (Sec. 4). The main significance and advantages of the proposed approach are emphasized through our example including a graph which models the human brain, and signals which reflect neural activity (Sec. 5). We conclude with open questions and further possibilities to refine the described framework (Sec. 6).

## 2. BACKGROUND

### 2.1 Graph Signal Processing Framework

Graphs provide an invaluable mathematical model of real-world networks for analyzing data on an irregular domain. They constitute a pair of the set  $\mathcal{V}$  of  $N$  vertices usually labeled as  $\mathcal{V} = \{1, 2, 3, \dots, N\}$ , and the set  $\mathcal{E}$  of edges denoted with tuples  $(i, j)$  when there is an edge between the  $i^{\text{th}}$  and  $j^{\text{th}}$  vertex and weights  $a_{ij}$ . Edge weights together build the adjacency matrix  $\mathbf{A}$  of size  $N \times N$  with entries  $a_{ij}$ . Graph signal is defined as a set of scalar values associated with each node of the graph, are then processed taking into account the underlying graph edges.<sup>4</sup> This framework is built upon the graph Laplacian matrix  $\mathbf{L} = \mathbf{D} - \mathbf{A}$ , where  $\mathbf{D}$  is the diagonal degree matrix with entries  $d_{ii} = \sum_{j=1}^N a_{ij}$ . A vector  $\mathbf{x}$  of size  $1 \times N$  corresponds to the graph signal (for a fixed chosen node labeling/ordering) and its graph Fourier transform (GFT) pair is further defined as

$$\hat{\mathbf{x}} = \mathbf{U}^{\top} \mathbf{x} \quad \text{and} \quad \mathbf{x} = \mathbf{U} \hat{\mathbf{x}}, \quad (1)$$

where  $\hat{\mathbf{x}}$  is the vector of spectral coefficients, and  $\mathbf{U}$  is the eigenbasis matrix containing orthogonal eigenvectors of  $\mathbf{L}$  as its columns, with respect to the eigendecomposition  $\mathbf{L} = \mathbf{U} \mathbf{\Lambda} \mathbf{U}^{\top}$ . Assuming the eigenvectors are ordered by increasing eigenvalues, a low pass filtered (with cutoff “frequency” at the  $w^{\text{th}}$  eigenvector) signal equals  $\mathbf{y} = \mathbf{U} \mathbf{H} \mathbf{U}^{\top} \mathbf{x}$ , where  $\mathbf{H}$  is a diagonal matrix with first  $w$  entries equal to 1 and others to 0.

In this context, the graph Laplacian matrix  $\mathbf{L}$  is the chosen matrix for a more general operator called the shift  $\mathbf{\Sigma}$ .<sup>1</sup> This operator allows to define a space of polynomial filters whose implementation in the vertex domain is highly beneficial from the computational point of view, as an eigendecomposition of a large matrix is time- and memory-consuming. With an assumption of a distinct set of matrix eigenvalues, every shift-invariant (commuting with the shift matrix) filter can be found as a polynomial of the shift operator<sup>11</sup>  $p(\mathbf{L})$  where the polynomial  $p$  is designed (often using Chebyshev recursion) to approximate the cutoff characteristic of the filter’s response in the range of the relevant eigenvalues.

### 2.2 Graph Slepian

Approaching a different problem, one may wish to find signals which, for a given graph and its subgraph (denoted with diagonal selection matrix  $\mathbf{S}$  with entries 1 for nodes within the subgraph, and 0 otherwise), exhibit maximally concentrated energy in the subgraph while having a localized (bandlimited) spectrum (at the first  $w$  low-pass spectral components). These signals are known as the graph Slepian,<sup>5</sup> and derive from a more general class of prolate spheroidal functions in the time domain.<sup>7,12</sup> Graph Slepian are found by maximizing (over coefficients vector  $\hat{\mathbf{x}}$ ) the energy concentration criterion  $\mu$  or minimizing the modified embedded distance criterion  $\xi$ :<sup>6</sup>

$$\mu = \frac{\hat{\mathbf{x}}^{\top} \mathbf{W}^{\top} \mathbf{U}^{\top} \mathbf{S} \mathbf{U} \mathbf{W} \hat{\mathbf{x}}}{\hat{\mathbf{x}}^{\top} \hat{\mathbf{x}}} \quad \text{and} \quad \xi = \frac{\hat{\mathbf{x}}^{\top} \mathbf{\Lambda}_W^{1/2} \mathbf{W}^{\top} \mathbf{U}^{\top} \mathbf{S} \mathbf{U} \mathbf{W} \mathbf{\Lambda}_W^{1/2} \hat{\mathbf{x}}}{\hat{\mathbf{x}}^{\top} \hat{\mathbf{x}}}, \quad (2)$$

\*Certain authors prefer to use the adjacency matrix directly to define graph signal operators.

where  $\mathbf{W}$  is a diagonal degree matrix with first  $w$  entries equal to 1, and  $\mathbf{\Lambda}_W = \mathbf{W}^\top \mathbf{\Lambda} \mathbf{W}$ . Hence, this reverts to finding the eigenvectors of the concentration matrix  $\mathbf{C} = \mathbf{W}^\top \mathbf{U}^\top \mathbf{S} \mathbf{U} \mathbf{W}$  or the modified concentration matrix  $\mathbf{C}_{emb} = \mathbf{\Lambda}_W^{1/2} \mathbf{C} \mathbf{\Lambda}_W^{1/2}$ , and subsequently calculating Slepian vectors as  $\mathbf{x}_k = \mathbf{U} \hat{\mathbf{x}}_k$  for  $k = 1, \dots, w$ . Even though both Slepian designs ( $\mu$  and  $\xi$ ) share the properties of vertex-domain localization and spectral bandlimitedness, the key difference between them lies in the notion of smoothness. Whereas  $\xi$ -Slepian signals are found as smooth and localized,  $\mu$ -Slepian signals are lacking this constraint as their energy is locally concentrated regardless of what is the oscillatory origin of that energy.

### 3. SLEPIAN GUIDED GRAPH SIGNAL FILTERING

The main question being explored in this paper is whether it is beneficial to define graph signal filtering and signal's spectral representation through the Slepian vectors as an orthogonal basis. Mathematically, if we have graph Slepian signals derived using the two criteria in Eq. (2) and stored in matrices  $\mathbf{U}_\mu$  and  $\mathbf{U}_\xi$ , respectively, of sizes  $N \times w$ , then for a signal  $\mathbf{x}$  we can define the  $\mu$ -Slepian GFT pair as:

$$\hat{\mathbf{x}} = \mathbf{U}_\mu^\top \mathbf{x} \quad \text{and} \quad \mathbf{x} = \mathbf{U}_\mu \hat{\mathbf{x}}, \quad (3)$$

and the  $\xi$ -Slepian GFT pair as

$$\hat{\mathbf{x}} = \mathbf{U}_\xi^\top \mathbf{x} \quad \text{and} \quad \mathbf{x} = \mathbf{U}_\xi \hat{\mathbf{x}}. \quad (4)$$

Note that these transforms are “almost unitary”. The columns of  $\mathbf{U}_\mu$  and  $\mathbf{U}_\xi$  are orthonormal, but mapping from  $\mathbf{x}$  to  $\hat{\mathbf{x}}$  reduces data dimensionality, *i.e.* the size of  $\hat{\mathbf{x}}$  is  $w \times 1$  and  $w < N$ . Hence the vector norm is not preserved entirely and this depends on the choice of  $w$ . Indeed, the total power of the spectral representation  $\hat{\mathbf{x}}$  accounts for  $(100 \cdot w/N)$  percent of the power of  $\mathbf{x}$ . Even though a certain amount of information is lost with this transform, it was shown that Slepian vectors are useful for exploring localized behavior. Indeed, for broadband signals, a local excerpt/subgraph (in time/graph domain) of the signal may not include all the spectral components and thus actually be bandlimited.

Once GFT has been defined, we can proceed to construct operators for graph signal processing. Here we explore only one – filtering. In the analysis performed in Sec. 5 only spectral domain filtering was performed, though we will give certain notes on the vertex domain filtering. A filtered signal  $\tilde{\mathbf{x}}$  is derived from  $\mathbf{x}$  through spectral domain as:

$$\tilde{\mathbf{x}} = \mathbf{U}_\square \mathbf{H} \mathbf{U}_\square^\top \mathbf{x}, \quad (5)$$

where  $\square$  can stand for either  $\mu$  or  $\xi$  for a given value of  $w$  and a fixed subgraph of interest (represented in the selection matrix  $\mathbf{S}$  when deriving Slepian vectors). Depending on the diagonal filter response matrix  $\mathbf{H}$  we can have a low pass filter (with nonnegative entries in the top left corner and zeros elsewhere), or a high pass filter (with nonnegative entries in the bottom right corner and zeros elsewhere). The terminology assumes ordering of eigenvectors according to decreasing  $\mu$  and increasing  $\xi$ . The size of  $\mathbf{H}$  is  $w \times w$ , so in this case the “high”- $\xi$  frequencies may still appear smooth if  $w \ll N$ . They are only high w.r.t. to the bandwidth extracted by the Slepian basis. Eq. 5 shows the analogy with the multiplication property of the Fourier transform. Indeed, the filtered output graph signal is derived after calculating the GFT of the input ( $\mathbf{U}_\square^\top \mathbf{x}$ ), multiplying with the frequency response of the filter ( $\mathbf{H}$ ) and finally taking the inverse GFT of the result (multiplying with  $\mathbf{U}_\square$ ).

As mentioned in Sec. 3, linear shift-invariant filters operating in the vertex domain as shift matrix polynomial multiplication  $\tilde{\mathbf{x}} = p(\mathbf{\Sigma})\mathbf{x}$  correspond to spectral domain filtering defined through eigenvectors of the shift matrix. In the case of Slepian bases  $\mathbf{U}_\mu$  and  $\mathbf{U}_\xi$ , the shift operator corresponds to expressions of concentration matrices  $\mathbf{U} \mathbf{C} \mathbf{U}^\top$  and  $\mathbf{U} \mathbf{C}_{emb} \mathbf{U}^\top$ , respectively, which for full bandwidth ( $w = N$ ) revert to the selection matrix  $\mathbf{S}$ , and selection modified Laplacian  $\mathbf{L}^{1/2} \mathbf{S} \mathbf{L}^{1/2}$ . Note that the calculation of Slepian vectors usually considers a column-truncated  $\mathbf{U}$  instead of indicator matrix  $\mathbf{W}$  applied to  $\mathbf{U}$ , in order to get concentration matrices of sizes  $w \times w$ , thus speeding up the subsequent eigendecomposition. However, if we use  $\mathbf{C}$  and  $\mathbf{C}_{emb}$  to find the shift operators,

we need to comply with dimensionality condition for matrix-vector multiplication and use indicator matrices to build  $\mathbf{C}$  and  $\mathbf{C}_{emb}$  of size  $N \times N$  as in Eq. 2.

The condition for a distinct set of eigenvalues of  $\mathbf{\Sigma}$  cannot be ignored,<sup>11</sup> which calls for a cautious definition of Slepian guided filtering. In general, there are around as many  $\mu$  eigenvalues equal to 1 as there are nodes in the selected subgraph for close to full bandwidth. Indeed, for bandlimited decomposition this number reduces but there may still exist a degenerate subspace (corresponding to  $\mu = 1$  with multiplicity strictly greater than 1) of the concentration matrix. Similarly, there is a degenerate subspace  $\xi = 0$  whose dimensionality depends on the size of the subgraph and the bandwidth. Hence, if we consider concentration matrices as shift operators, there may be spectral domain operators that do not have their analogues in the vertex domain, at least not in the class of polynomial-shift operators. In order to make sure that the spectral filter can be represented as  $p(\mathbf{C})$  (or  $p(\mathbf{C}_{emb})$ ), the same value of entries of  $\mathbf{H}$  must be used for all spectral components spanning the same eigenvalue subspace. In practice, this means that one should be particularly careful for  $\mu$ -Slepian filtering as there may even exist two degenerate subspaces at far ends ( $\mu = 1$  and  $\mu = 0$ ) so that the filtering cutoff frequency (eigenvector index) is only “allowed” in the mid-band. The situation is somewhat simpler in the case of  $\xi$ -Slepian guided filtering since the only degenerate subspace is at the low end ( $\xi = 0$ ), so that we can just perform high-pass filtering while choosing the cutoff eigenvector inside the strictly positive range  $\xi > 0$ .

#### 4. POWER SPECTRUM DENSITY ESTIMATION ON RANDOM GRAPHS

Spectral domain representation of a graph signal provides insight into oscillatory patterns of the signal along the neighboring nodes of the graph. Connectivity of the graph nodes is employed by using the Laplacian matrix to define GFT, hence incorporating the geometrical/topological properties of the graph. However, as we show in the following example, certain signal behavior may remain hidden in the noise and appear to have a spectrum corresponding to a random signal. The approach of defining the spectral domain with Slepian eigenbasis allows to properly differentiate between these types of behavior. We decided to use random graphs and estimate power spectrum density of signals defined on their vertices in order to show how the Slepian eigenbasis overcomes the problem existing in the case of the Laplacian spectrum.

An ensemble of 10000 Erdős–Rényi random graphs<sup>13</sup> with  $N = 100$  nodes and edge probability  $p = 0.2$  was generated. Furthermore, for each of them, an instance of three types ( $s_1$ ,  $s_2$ , and  $s_3$ ) of random signals was generated on the vertices. Signal  $s_1$  is a zero-mean unit-norm random signal with uniformly distributed values. Signal  $s_2$  is uniformly distributed, has zero mean and unit norm, and its values within the subset of 50 nodes (right semicircle in Fig. 1) exhibit higher variance than values on the rest of the vertices. Signal  $s_3$  is similar to  $s_2$  but with only the mean being different between the two subsets of nodes. One instance of each of the three signals is illustrated in Fig. 1 with the underlying graph.

In analogy with periodogram of time series, the power spectrum density of graph signals are estimated as the average (over the ensemble of pairs graph/signal) of the spectral powers, *i.e.*, element-wise square magnitude of the GFT of signals. In order to compare the proposed approach with the existing one, we repeated this for three definitions of GFT: using full Laplacian eigenbasis (100 eigenvectors),  $\mu$ -Slepian eigenbasis (75 eigenvectors due to chosen finite bandwidth  $W = 75$ ), and  $\xi$ -Slepian eigenbasis (75 eigenvectors). The PSDs are plotted in blue, red, and cyan lines, respectively, assuming the ordering of spectral components w.r.t. increasing eigenvalues for Laplacian eigenvectors and  $\xi$ -Slepians, and decreasing eigenvalues for  $\mu$ -Slepians (Fig. 1, bottom row). Note that due to  $W = 75$  and the number of nodes in the subgraph being 50, the spectral bands encompass 25 eigenvalues  $\xi = 0$ , 25 eigenvalues  $\mu = 0$  (both gray shaded areas), and 25 eigenvalues  $\mu = 1$  (yellow shaded area). We also explored how the PSD estimates degrade if the selection matrix in the definition of Slepian basis does not accurately target the nodes of the subgraph which indeed exhibits localized behavior. We shifted the selection for 20% (10 nodes) around the topological circle of the graph representation (Fig. 1), therefore excluding 10 nodes with relevant subgraph behavior and including 10 irrelevant ones. These PSD estimates are presented in Fig. 1 with dashed magenta line ( $\mu$ -Slepian basis) and dashed green line ( $\xi$ -Slepian basis).

Evidently, Laplacian PSD does not differentiate between  $s_1$ ,  $s_2$ , and  $s_3$ . All three have broadband and almost flat PSDs (note the corresponding ranges of values in Fig. 1) which is expected knowing that the signal is (globally) random. Even though the special localized properties in the context of mean ( $s_3$ ) and variance ( $s_2$ )

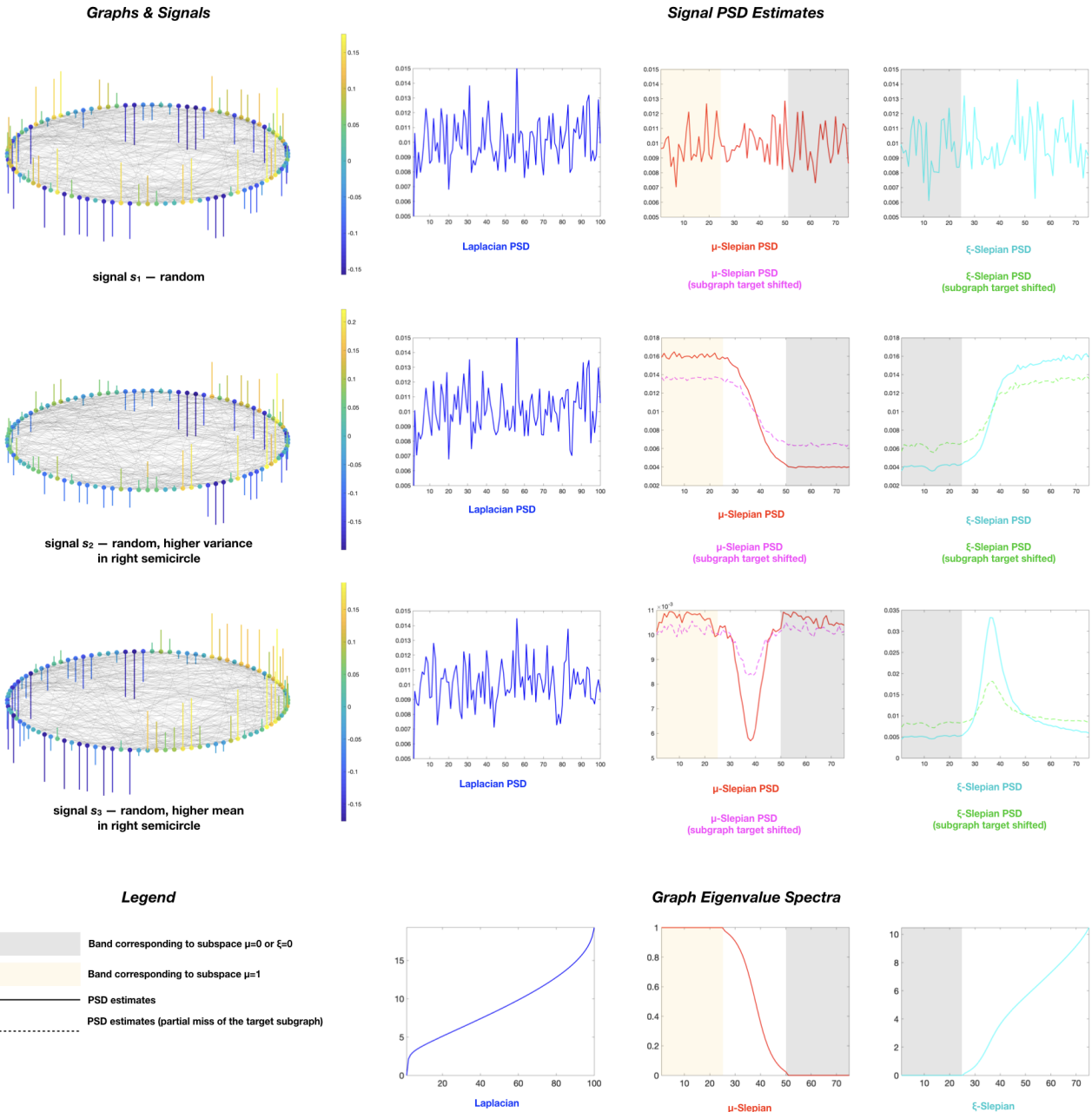


Figure 1. On the left: an instance of random graph ( $N = 100$ ) and three different signals with values encoded by color and length of vertical lines:  $s_1$  - a random signal,  $s_2$  - random signal with higher variance on the nodes forming the right semicircle of the topology,  $s_3$  - random signal with higher mean on the nodes forming the right semicircle. On the right: PSD estimates of these types of signals defined as the average power spectrum over an ensemble of 10000 graph/signal pairs defined with Laplacian (blue),  $\mu$ -Slepians (red and magenta), and  $\xi$ -Slepians (cyan and green). In the case of Slepian bases, the solid lines (red, cyan) correspond to cases when the selection matrix accurately extracts the right semicircle nodes, whereas dashed lines (magenta, green) correspond to cases where the selection is shifted by 20% of the number of nodes in the relevant subgraph. The shaded areas represent the spectral bands defined by the high-multiplicity eigenvalue equal to 0 (gray) or 1 (yellow). For visual clarity, plots of Laplacian spectra are zoomed around 0.01 at  $y$ -axis so that the first component (with eigenvalue equal to 0) cannot be seen, but as it reflects the global signal mean, it is equal to 0 in all instances. The plots in the last row represent the mean graph eigenvalue spectrum for each of the three used bases.

are introduced in the half of the vertex-domain of the signal, the Laplacian approach is not powerful enough to grasp this kind of signal behavior. Furthermore, the random signal  $s_1$  shows Slepian-based PSDs with the same features (broadband, almost flat) confirming that the signal  $s_1$  is indeed random (top row in Fig. 1).

On the other hand,  $\mu$ - and  $\xi$ -Slepian PSDs of  $s_2$  and  $s_3$  are different from the one of the random signal  $s_1$ , as well as from each other. As expected, Slepian eigenvectors are able to extract relevant information on localized signal behavior. Energy concentration Slepian PSD of  $s_2$  has higher values in range  $\mu = 1$ , lower in  $\mu = 0$ , and the density is decreasing in the middle, in overall resembling the (scaled) eigenvalue spectrum of the corresponding concentration matrix. The  $\mu$ -Slepian PSD of  $s_3$  exhibits a different shape, having high values in both extremal eigenvalue ranges, with a significant trough in the middle band. As compared to the PSD estimate of  $s_1$ , this suggests that the difference of local signal variance is encoded in reducing the relative contribution of nonconcentrated spectral components ( $\mu \approx 0$ ). Since the variance of the signal is indeed locally diminished in the unselected subgraph, that is where the “nonconcentrated” components exist. Furthermore, reducing the local mean in the unselected subgraph reduces the contribution of the spectral band  $0 \ll \mu \ll 1$ , which in general consists of components concentrated in both selected and unselected subgraphs. If we represent the difference of local means as a piecewise-constant signal over the two subgraphs, it becomes more intuitive that this feature would be encoded in the class of equally concentrated and nonconcentrated signals, *i.e.* those existing in the midband of  $\mu$ .

Significant differences of PSDs of  $s_2$  and  $s_3$  are also present in the case of  $\xi$ -Slepian eigenbasis. Signal  $s_2$  exhibits low contribution of smooth low-frequency (low modified embedded distance) spectral components. Indeed, variance in the selected subgraph is higher relative to the rest of the graph, so one should not expect smooth components in the Slepian spectrum. On the other hand, PSD of  $s_3$  as compared to that of  $s_1$  exhibits an increase of the middle frequency components, seen as a prominent peak in the mid-spectrum. This can be explained similarly as in the case of  $\mu$ -spectrum. A piece-wise constant signal can hardly be classified as neither smooth or nonsmooth, but rather as piecewise-smooth, hence it is explained by components corresponding to moderate values of  $\xi$ .

The ability to extract otherwise hidden signal behavior makes the Slepian GFT basis a powerful tool for detection of localized processes on graphs. Even in cases when the selection matrix does not accurately (with 20% of subgraph nodes missed) target the subgraph of interest (dashed magenta and green PSDs in Fig. 1), the spectral contents of the signals are distinct enough to suggest an existing discrimination between the explored types of graph signals. This result points to a potential benefit of processing signals with Slepian-defined GFT – manipulation of signals with complex behavior which exist on segregation-modeled graphs (with partial a priori knowledge of meaningful subgraphs). Hence, in the next section, we explore graph signal filtering in Slepian spectral domain.

## 5. GUIDED FILTERING OF BRAIN SIGNALS

Neuroscience has particularly advanced since the development of graph-based methods and GSP.<sup>14,15</sup> Exploring the human brain using graph models allowed for high-level abstraction approaches thus simplifying the complexity of the problem at hand. By parceling the brain into relevant regions of interest one can analyze segregation/integration levels of both anatomical and functional nature.<sup>16</sup> The two most common approaches are to build a graph by connecting anatomically linked regions (as nodes) as derived from diffusion weighted imaging,<sup>17</sup> or by connecting regions with correlated time courses of BOLD (Blood-Oxygenation-Level-Dependent<sup>18</sup>) signals recorded in these regions with functional magnetic resonance imaging (fMRI).<sup>19</sup> Efforts to jointly explore both structure and function of the brain<sup>20–22</sup> have been recently boosted by GSP techniques through building a graph out of anatomical connections, but processing BOLD signals residing on that graph in order to examine how the dynamics of neural activity are aligning with the underlying structure.<sup>15,23</sup> Here, we follow this joint approach.

The dataset we use in the following examples consists of publicly available Human Connectome Project<sup>24,25</sup> structural and functional MRI recordings of the human brain. We constructed a weighted graph representing neural pathway strengths between 360 brain regions<sup>26</sup> for 21 subjects and averaged the results into a unique graph for all available subjects. The BOLD signals (sampling rate 0.72 Hz, duration approx. 5 min) acquired from fMRI were averaged over voxels belonging to the same region/node and z-scored, resulting in a signal

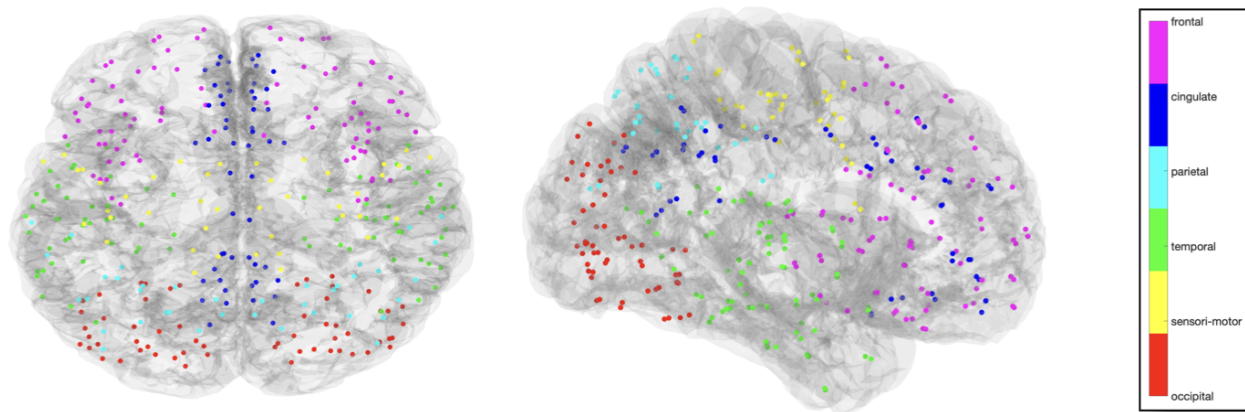


Figure 2. Subgraphs for focusing Slepian designs. Nodes of subgraphs are color-coded according to the regions based on anatomical and functional segregation of the human brain. These are occipital (red), sensori-motor (yellow), temporal (green), parietal (cyan), cingulate (blue), and frontal (magenta) regions.

matrix of size  $360 \times 395$  per subject; *i.e.* we have as many graph signals as there are time points in the functional data. The signals were recorded while subjects performed a working memory task involving visual stimuli.<sup>24</sup> Furthermore, we acquired resting-state BOLD signals in matrices of size  $360 \times 1990$  per subject.

In order to justify the Slepian guided filtering in the context of the available dataset, we have performed a PSD estimation analysis analogous to the random graph analysis in Sec. 4. The subgraphs for focusing graph Slepian were chosen according to the general knowledge on structural and functional neuroanatomy (Fig. 2). These are occipital (58 nodes), sensori-motor (42 nodes), temporal (82 nodes), parietal (38 nodes), cingulate (54 nodes), and frontal (86 nodes) regions. For each of the subgraphs and the two Slepian designs ( $\mu$  and  $\xi$ ), we have averaged the power spectra based on Slepian eigenbasis over all time points per subject, considering separately resting-state and task-based signals. The resulting eigenvalue spectra of the Slepian ( $\mu$  and  $\xi$ ) and Laplacian ( $\lambda$ ) bases are shown in Fig. 3, whereas the final PSD estimates are plotted in Fig. 4 (full and dashed lines denote median across subjects, and the shaded dark gray areas reflect the 25<sup>th</sup> and 75<sup>th</sup> percentiles). All Slepian signals were designed with bandwidth  $W = 100$  so that  $W$  is higher than the maximal number of nodes in a focused subgraph, thus making sure the spectra would encompass both degenerate and non-degenerate subspaces.

Comparing the PSD estimates to those of random graph signals in Fig. 1 reveals certain similar shapes. Higher contribution of components in range  $\mu \gg 0$  than in  $\mu = 0$  are evident in all  $\mu$ -PSDs with the clear split coinciding with nonzero and zero eigenvalues for the cases of occipital and cingulate areas. This reflects variance of a graph signal higher in the focused subgraph than in the rest of the graph. The same behavior is confirmed in the frontal regions in task by  $\xi$ -Slepian PSD having a higher contribution of the non-degenerate subspace than the subspace  $\xi = 0$ . On the other hand, difference of local mean is encoded by higher contribution of components with  $\xi$  close but not equal to 0 than by the rest of the spectrum (Fig. 1). To a certain extent, this behavior is reflected by a concave arc-shaped trend of PSD estimates in the case of occipital and temporal subgraphs. Apparent feature (spatial localization) of graph signals living on the brain network model introduce a caveat for Laplacian graph signal filtering. As in the example including random graphs, one could expect certain signal behaviors to remain hidden from the Laplacian spectra and thus not be suitable to filtering in a conventional GSP manner.<sup>4</sup> This motivated us to perform Slepian guided graph signal filtering on the available dataset and check whether there is any information accessed by the Slepian and missed by the graph Laplacian approach.

We performed graph signal filtering of task-based data using Laplacian spectra as described in Sec. 2.1 and using  $\mu$  and  $\xi$  Slepian spectra as in Eq. 5. Filters were designed as ideal spectral domain operators (values of  $\mathbf{H}$  are binary). In the case of Laplacian filtering we defined a low pass filter preserving components for which  $\lambda \leq 4$  resulting in  $W = 34$ . In the case of Slepian filtering, the bandwidth of Slepian eigenvectors was  $W = 100$ ,

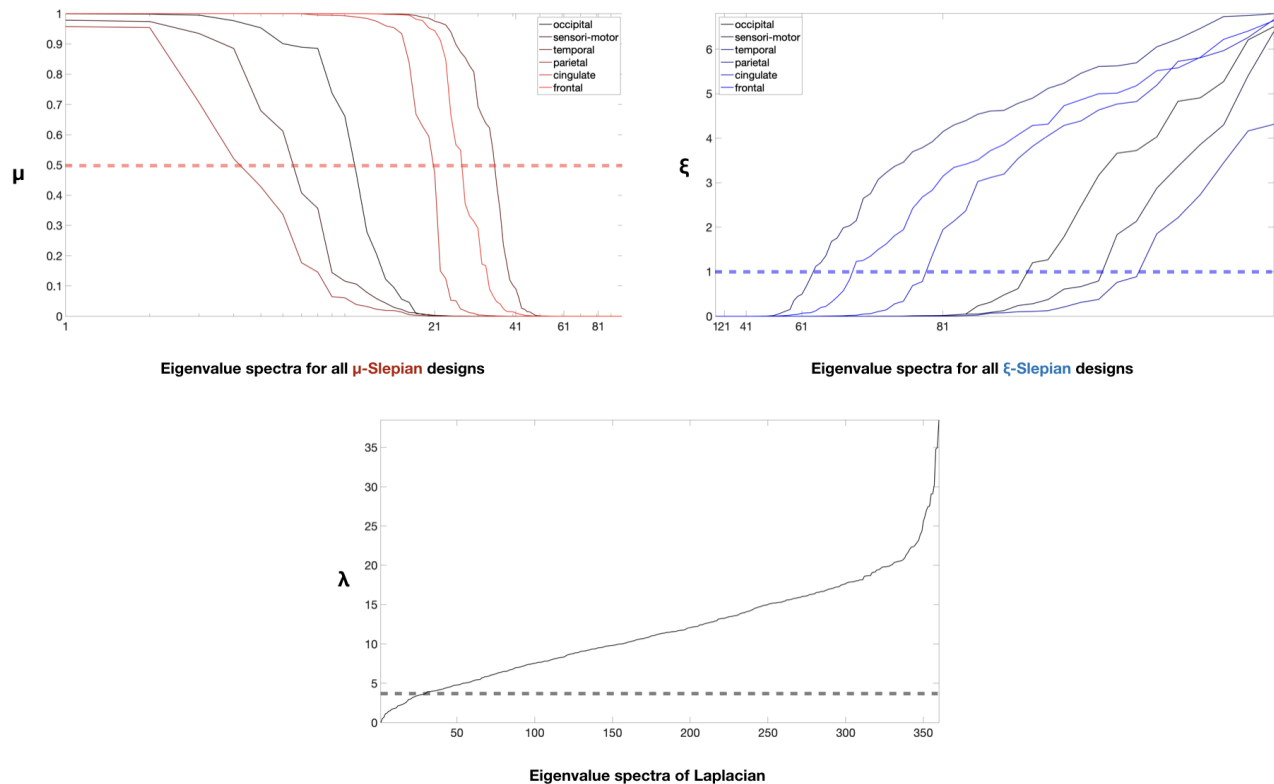


Figure 3. Eigenvalue spectra for  $\mu$ - (top left),  $\xi$ -Slepian (top right) and Laplacian eigenbasis (bottom). Different shades of red ( $\mu$ ) and blue ( $\xi$ ) denote cases when Slepian are concentrated in different subgraphs (labeled in the legend). For clarity  $x$ -axes are in log-scale for Slepian designs. Horizontal dashed lines cross the spectra at points used as cutoff frequencies of filters used in the example in Fig. 5. These result in cutoff eigenvector indices (ordered as subgraphs in the legend from top to bottom): 11, 7, 34, 4, 21, and 26 for  $\mu$ -Slepian, and 12, 8, 36, 6, 21, and 30 for  $\xi$ -Slepian, and 34 for Laplacian filtering.

whereas the filter passband widths were set to include components at least as concentrated as  $\mu \geq 0.5$  and at most as smooth as  $\xi \geq 1$  (see dashed lines in Fig. 3). This way, the cutoff frequency of all filters was chosen so that it is not splitting any of the degenerate subspaces ( $\mu = 1$ ,  $\mu = 0$ , or  $\xi = 0$ ), thus complying to the shift-enabled condition,<sup>11</sup> *i.e.* the passband always includes the whole subspace  $\mu = 1$ , and always excludes all the spectral components in the subspaces  $\mu = 0$  and  $\xi = 0$ . Values of the cutoff eigenvector indices  $\Omega$  are: 11, 7, 34, 4, 21, and 26 for  $\mu$ -Slepian, and 12, 8, 36, 6, 21, and 30 for  $\xi$ -Slepian, and 34 for Laplacian filtering (ordered as subgraphs in Fig. 4 from top to bottom). The passbands are marked with red, blue, and dark gray flags above PSD estimates in Fig. 4. We note that although the idea of Slepian guided graph signal filtering was briefly introduced in Ref. 15 for the purpose of surrogate-based signal excursions analysis, this condition for valid shift-invariant filters was not previously considered.

Inspection of the filtered signals was done in terms of the known experimental task paradigm of the fMRI recordings. After filtering graph signals at all time points for all subjects, we reconstructed the BOLD time series and explored how well they reflect subject's response to the task stimuli. Results are given in Fig. 5. We present the outcomes of 3 cases guiding the Slepian vectors to the occipital, temporal, and cingulate subgraph (from top to bottom in Fig. 5). For each subject's filtered (and non-filtered) BOLD time courses we calculated the mean signal over all nodes in the corresponding subgraph. The plots in Fig. 5 then show the median (solid lines) and the range between 25<sup>th</sup> and 75<sup>th</sup> percentile (gray shaded areas) over all 21 subjects. Here we chose the median instead of mean as a more robust metric in order to account for the heterogeneous nature of the neuroimaging data across different people. We compared these median signals for all filtering cases: Laplacian,

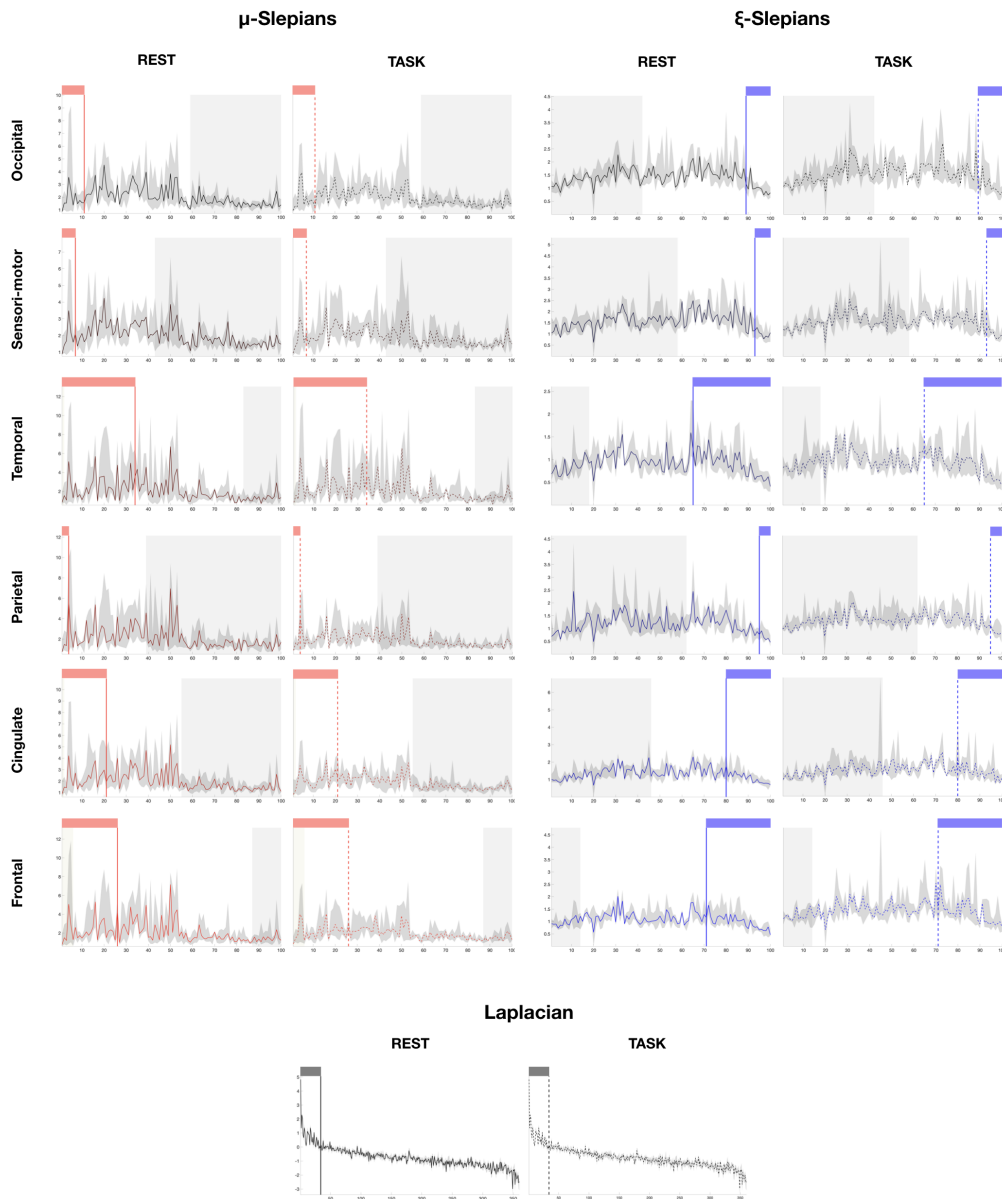


Figure 4. Power spectrum density estimates (averaged over available time points) of brain graph signals calculated using Slepian GFT focused on 6 subgraphs: (from top to bottom) occipital, sensori-motor, temporal, parietal, cingulate, and frontal region (see Fig. 2), and using Laplacian eigenbasis (bottom middle). The estimation was performed separately for Laplacian,  $\mu$ - (left) and  $\xi$ -Slepians (right), and for resting-state and task-based BOLD time courses (in the appropriately labeled columns). Zero-eigenvalue subspaces are denoted with light gray shaded areas and degenerate  $\mu = 1$  subspaces with yellow shaded areas. Dark gray shaded areas reflect 25<sup>th</sup> and 75<sup>th</sup> percentiles of PSD estimates over subjects. Bandwidth of Slepian signals was set to  $W = 100$ . Red, blue, and dark gray flags mark the passbands of filters used in the following example in Fig. 5.

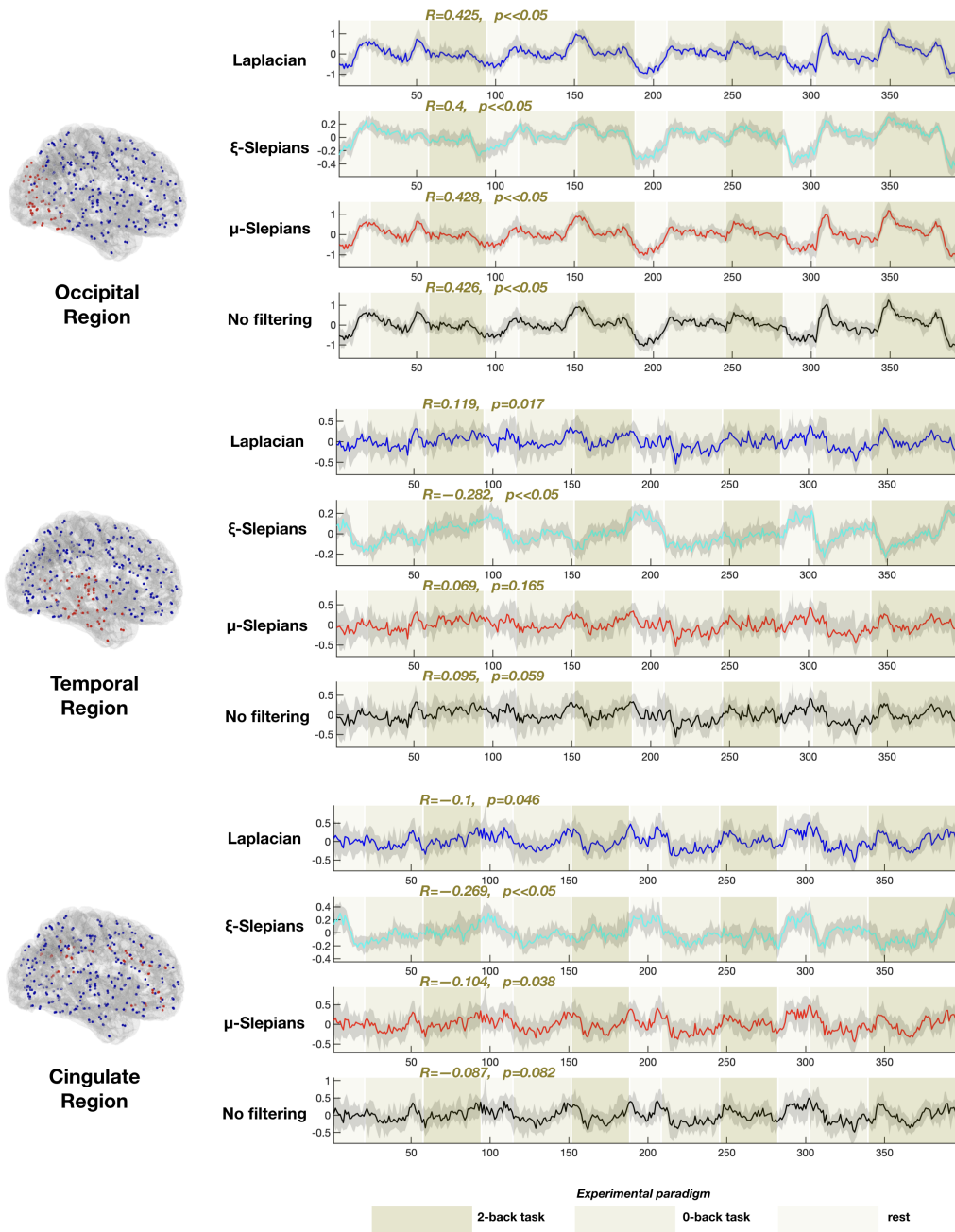


Figure 5. Mean (over nodes in a subgraph) task-based BOLD signals before (black lines) and after graph filtering (blue lines: Laplacian, cyan lines:  $\xi$ -Slepian, and red lines:  $\mu$ -Slepian). The lines denote median signal over 21 subjects with the shaded areas around representing the range between 25<sup>th</sup> and 75<sup>th</sup> percentiles. The shades of yellow follow the task paradigm from bright to dark color denoting fixation time, 0-back task and 2-back task. Values of correlation coefficient  $R$  (and corresponding  $p$ -value) between the median signals and 2-back task paradigm (convolved with HRF) are reported in dark yellow font. The results are shown for 3 subgraphs: (from top to bottom) occipital, temporal, and cingulate regions.

$\xi$ -Slepian,  $\mu$ -Slepian, and no (allpass) filtering. In each case we report the correlation coefficient  $R$  (and the corresponding  $p$ -value) with the binary indicator function of the 2-back working memory task<sup>†</sup>. In order to emphasize (dis)similarity between the two, in Fig. 5 we reflect the full task paradigm in time as shaded areas with light to dark yellow background colors denoting fixation (rest), 0-back, and 2-back task, in that order.

In the occipital region, values of  $R$  indicate a moderate positive and statistically significant correlation (above 0.4) regardless of the chosen filtering. Since the task in question includes visual stimuli (images were shown to subjects as a part of the working memory task<sup>24</sup>), one would indeed expect to capture neural activity following the paradigm in the occipital region, as it is known that visual processing in the human brain is highly localized in this area. However, focusing on the occipital subgraph does not show the advantages of using Slepian guided filtering over other approaches. Here it was included to emphasize the fact that the choice of the appropriate type of filtering should be guided by the nature of the graph and of the subgraph of interest. On the other hand, in the case of temporal and cingulate subgraphs, all types of filtering except  $\xi$ -Slepian exhibit very low (up to 0.1 in absolute value) and/or statistically insignificant value of  $R$ . In fact, Laplacian filtering gives somewhat higher and significant  $R = 0.119$ , but this may be attributed to a response to acoustic noise, since fMRI recordings are very loud and the auditory processing is localized in the temporal lobe of the human brain.<sup>28</sup> Still,  $\xi$ -Slepian filtering manages to extract significant negative correlation ( $R = -0.282$ ) of the mean BOLD signal in the temporal region, as well as in the cingulate subgraph ( $R = -0.269$ ). This result has not been put forward by the other approaches even though it might have been anticipated from the neuroscientific point of view. In fact, a similar filtering approach repeated on a finer scale with 22 nonoverlapping brain regions<sup>26</sup> has revealed that the biggest contributors to this “correlation boosting” are the lateral temporal and posterior cingulate regions. These are parts of the so called default mode network (DMN)<sup>29</sup> which represents a pattern of brain regions known to often exhibit neural activity negatively correlated with whatever task is being performed by the subject. Hence, the only way one can confirm the “presence” of the activity in these parts of the DMN at smooth frequencies (low-pass bandlimited behavior) is by employing  $\xi$ -Slepian guided filtering. Energy concentration based Slepian do not show clear advantages in this example, except just slightly higher  $R$  and lower significant  $p$  value (for alpha level 0.05) in the case of the cingulate region, as compared to no filtering. However, the structured shape of  $\mu$ -based PSD estimates in Fig. 4 do indicate that there may still be an application where this type of Slepian would be invaluable.

The ability of  $\xi$ -Slepian basis to extract information otherwise inaccessible by classical graph signal filtering could be partially understood as a consequence of the specific graph connectivity pattern. The main difference between Laplacian eigenvectors and  $\xi$ -Slepian signals lies in the localization property. Laplacian eigenvectors reflect signals changing smoothly across nodes with highly weighted edges connecting them, and nonsmoothly across loosely connected or disconnected nodes. In this context, for a given bandwidth  $W$ , a lowpass Laplacian filter can extract globally smooth signals across the whole graph. However, if a signal is locally smooth across a certain subgraph, and outside it is either nonsmooth or smooth but in an anticorrelated fashion, this type of behavior would be considered high frequency by the graph Laplacian. Note that this is the case in the example of the cingulate region (Fig. 6). Cingulate subgraph is loosely connected to the whole graph, and just slightly more connected to the frontal region. We would expect both cingulate and frontal region activity to be correlated with the task indicator function, with negative and positive coefficient values, respectively (cingulate as it includes part of the DMN, and frontal as it is generally linked to human cognitive function). However, despite this smooth behavior, it is anticorrelated across the border between these two subgraphs, and it is detected as high frequency by the Laplacian, thus being cut off during filtering. On the other hand, the nature of Slepian designs includes the notion of localized behavior, whereas the  $\xi$  criterion exactly optimizes for locally smooth patterns inside the selected subgraph. Hence, for the same bandwidth  $W$ , Slepian basis preserves the task anticorrelated behavior in the cingulate region as it is considered low frequency. The same holds for the case of focusing on the temporal subgraph. Indeed, temporal subgraph is highly connected to the occipital and frontal regions where we identify positive correlation with the task. As a consequence, even a small amount of task-negatively correlated activity in the temporal region renders the pattern globally high frequency as seen by the graph Laplacian. Nonetheless,

---

<sup>†</sup>More precisely we used the binary indicator convolved with haemodynamic response function (HRF) mathematically modeled with gamma functions. HRF is used to account for the time delay between the actual neural response to stimulus and the cardiovascular response proxy that is in fact being captured by fMRI.<sup>27</sup>

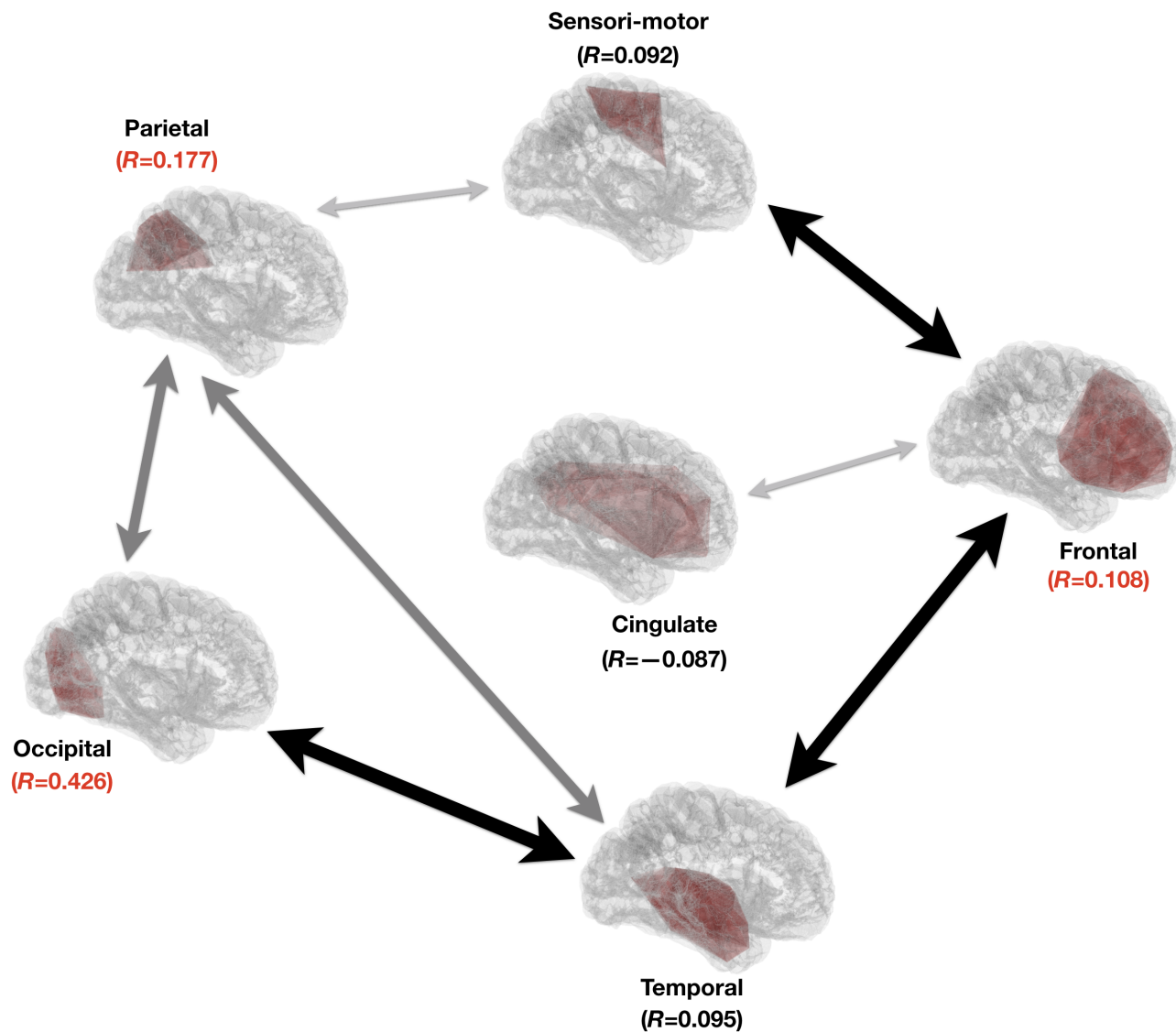


Figure 6. Illustration of the brain graph based on anatomical connections. The 6 subgraphs used in Slepian designs are shown in red. The total strength of all edges between nodes in two subgraphs is encoded in the width and color of an arrow line between the subgraphs. Edges (arrows) between the most weakly connected pairs of subgraphs are excluded. The values  $R$  at each subgraph indicate the correlation coefficient between the mean BOLD signal in the subgraph (nonfiltered) and the 2-back task paradigm. Significant values w.r.t. alpha level of 0.05 are colored in red.

$\xi$ -Slepian filtering successfully extracts this activity in the temporal lobe due to subgraph selection. Finally, in the case of occipital region, even Laplacian filtering does extract task-positively correlated activity. This may be explained by the fact that the same type of activity can be seen in the parietal region (known to be associated with the working memory) so that Laplacian in fact sees the occipital activity as a part of spatially larger pattern (including both occipital and parietal subgraphs moderately connected – see Fig. 6) which is supposedly big enough to be considered as a globally smooth pattern and thus be included in the filter's passband.

## 6. CONCLUSIONS AND FUTURE WORK

Slepian guided graph signal filtering benefits from the localization step by using a priori knowledge of meaningful subgraphs. This leads to the ability to extract localized bandlimited signal behavior that cannot be identified by the graph Laplacian due to its affinity for global patterns. Graph signal PSD estimation on both random and brain graphs have suggested a big amount of signal's information is stored in discrepancies between local activities. Furthermore, brain signal filtering example pointed to the importance of the underlying graph connectivity as it constrains what signal patterns can and cannot be detected by different techniques.

Still, there remain several open questions and possibilities to further extend our understanding and capabilities of graph Slepian in GSP. Energy concentration Slepian do show intriguing PSD estimates and yet no apparent uniqueness of the results in the case of filtering. This may be explained by the fact that our example explores the slow<sup>‡</sup> task paradigm, whereas  $\mu$ -Slepian do not take into account the smoothness of signals, but rather energy concentration regardless of what is its spectral nature. Hence, one of possible directions to search for an on-hands application of  $\mu$ -guided filtering could be in resting-state BOLD signals, since the nature of these is still widely unclear. In this context,  $\mu$ -Slepian may provide a generalized approach to finding localized intrinsic brain activity.

Joint extraction of both locally smooth and energy concentrated Slepian signals was recently proposed<sup>9</sup> as optimization of the criterion  $\mu - \xi$ . Extending this type of signals, called  $\zeta$ -Slepian, to the framework of guided graph signal filtering is certainly worth exploring. First, the joint criterion would search for more relevant signal behavior. Secondly,  $\zeta$ -Slepian are found by eigendecomposition of a polynomial of normalized adjacency matrix excluding any bandwidth parameter. This simplifies the filtering procedure since we would no longer have two parameters ( $W$  and  $\Omega$ ). Slepian bandwidth is implicitly defined, therefore the only free parameter is the filtering cutoff index  $\Omega$  (s.t.  $\Omega < N$ ).

Further in the context of neuroscience, the described Slepian filtering may find use on graphs known as functional connectomes. There, BOLD signals are considered both as graph signals and as basis to calculate the edge strengths between corresponding nodes w.r.t. to temporal coupling of the time series.<sup>14</sup> However, as a general framework, Slepian guided graph signal filtering is not constrained by a specific application domain. In all disciplines inclined towards GSP analysis, one could further benefit from guided filtering, *i.e.* geoscience and radar imaging,<sup>30</sup> sensor networks and smart grids,<sup>31</sup> image processing,<sup>32</sup> etc. Finally, before applying more sophisticated techniques, one should further elaborate on the theoretical aspect of the Slepian guided filtering, possibly by investigating the localization feature from a graph wavelet perspective.<sup>33,34</sup>

## ACKNOWLEDGMENTS

This work was supported in part by the Swiss National Science Foundation (project 200021\_175506).

## REFERENCES

- [1] Ortega, A., Frossard, P., Kovačević, J., Moura, J. M. F., and Vandergheynst, P., "Graph signal processing: Overview, challenges, and applications," *Proceedings of the IEEE* **106**, 808–828 (May 2018).
- [2] Sandryhaila, A. and Moura, J. M. F., "Discrete signal processing on graphs," *IEEE Transactions on Signal Processing* **61**, 1644–1656 (apr 2013).
- [3] Sandryhaila, A. and Moura, J. M. F., "Discrete signal processing on graphs: Frequency analysis," *IEEE Transactions on Signal Processing* **62**, 3042–3054 (jun 2014).
- [4] Shuman, D. I., Narang, S. K., Frossard, P., Ortega, A., and Vandergheynst, P., "The emerging field of signal processing on graphs: Extending high-dimensional data analysis to networks and other irregular domains," *IEEE Signal Processing Magazine* **30**, 83–98 (may 2013).
- [5] Tsitsvero, M., Barbarossa, S., and Lorenzo, P. D., "Signals on graphs: Uncertainty principle and sampling," *IEEE Transactions on Signal Processing* **64**, 4845–4860 (Sept. 2016).

<sup>‡</sup>Here the term slow refers to temporal smoothness. However, in the irregular setting such as graphs, temporal and spatial frequencies may have interdependencies strongly affecting the performed analysis.

- [6] Ville, D. V. D., Demesmaeker, R., and Preti, M. G., “When slepian meets fiedler: Putting a focus on the graph spectrum,” *IEEE Signal Processing Letters* **24**, 1001–1004 (July 2017).
- [7] Slepian, D. and Pollak, H. O., “Prolate spheroidal wave functions, fourier analysis and uncertainty - I,” *Bell System Technical Journal* **40**, 43–63 (Jan. 1961).
- [8] Tsitsvero, M. and Barbarossa, S., “On the degrees of freedom of signals on graphs,” (Sept. 2015).
- [9] Petrovic, M., Bolton, T. A. W., Preti, M. G., Liégeois, R., and Ville, D. V. D., “Guided graph spectral embedding: Application to the *c. elegans* connectome,” *Network Neuroscience* **3**, 807–826 (Mar. 2019).
- [10] Fortunato, S. and Hric, D., “Community detection in networks: A user guide,” *Physics Reports* **659**, 1–44 (Nov. 2016).
- [11] Chen, L., Cheng, S., Stankovic, V., and Stankovic, L., “Shift-enabled graphs: Graphs where shift-invariant filters are representable as polynomials of shift operations,” *IEEE Signal Processing Letters* **25**, 1305–1309 (Sept. 2018).
- [12] Slepian, D., “Prolate spheroidal wave functions, fourier analysis, and uncertainty - V: The discrete case,” *Bell System Technical Journal* **57**, 1371–1430 (May 1978).
- [13] Erdős, P. and Rényi, A., “On random graphs, I,” *Publicationes Mathematicae (Debrecen)* **6**, 290–297 (1959).
- [14] Huang, W., Goldsberry, L., Wymbs, N. F., Grafton, S. T., Bassett, D. S., and Ribeiro, A., “Graph frequency analysis of brain signals,” *IEEE Journal of Selected Topics in Signal Processing* **10**, 1189–1203 (oct 2016).
- [15] Huang, W., Bolton, T. A. W., Medaglia, J. D., Bassett, D. S., Ribeiro, A., and Ville, D. V. D., “A graph signal processing perspective on functional brain imaging,” *Proceedings of the IEEE* **106**, 868–885 (may 2018).
- [16] Sporns, O. and Betzel, R. F., “Modular brain networks,” *Annual Review of Psychology* **67**, 613–640 (Jan. 2016).
- [17] Bihan, D. L. and Iima, M., “Diffusion magnetic resonance imaging: What water tells us about biological tissues,” *PLOS Biology* **13**, e1002203 (July 2015).
- [18] Leonardi, N., Richiardi, J., Gschwind, M., Simioni, S., Annoni, J.-M., Schluep, M., Vuilleumier, P., and Ville, D. V. D., “Principal components of functional connectivity: A new approach to study dynamic brain connectivity during rest,” *NeuroImage* **83**, 937–950 (Dec. 2013).
- [19] Logothetis, N. K., “What we can do and what we cannot do with fMRI,” *Nature* **453**, 869–878 (June 2008).
- [20] Ajilore, O., Zhan, L., GadElkarim, J., Zhang, A., Feusner, J. D., Yang, S., Thompson, P. M., Kumar, A., and Leow, A., “Constructing the resting state structural connectome,” *Frontiers in Neuroinformatics* **7** (2013).
- [21] Becker, C. O., Pequito, S., Pappas, G. J., Miller, M. B., Grafton, S. T., Bassett, D. S., and Preciado, V. M., “Spectral mapping of brain functional connectivity from diffusion imaging,” *Scientific Reports* **8** (Jan. 2018).
- [22] Abdelnour, F., Dayan, M., Devinsky, O., Thesen, T., and Raj, A., “Functional brain connectivity is predictable from anatomic network’s laplacian eigenstructure,” *NeuroImage* **172**, 728–739 (May 2018).
- [23] Medaglia, J. D., Huang, W., Karuza, E. A., Kelkar, A., Thompson-Schill, S. L., Ribeiro, A., and Bassett, D. S., “Functional alignment with anatomical networks is associated with cognitive flexibility,” *Nature Human Behaviour* **2**, 156–164 (Dec. 2017).
- [24] Essen, D. V., Ugurbil, K., Auerbach, E., Barch, D., Behrens, T., Bucholz, R., Chang, A., Chen, L., Corbetta, M., Curtiss, S., Penna, S. D., Feinberg, D., Glasser, M., Harel, N., Heath, A., Larson-Prior, L., Marcus, D., Michalareas, G., Moeller, S., Oostenveld, R., Petersen, S., Prior, F., Schlaggar, B., Smith, S., Snyder, A., Xu, J., and Yacoub, E., “The human connectome project: A data acquisition perspective,” *NeuroImage* **62**, 2222–2231 (oct 2012).
- [25] Glasser, M. F., Sotiropoulos, S. N., Wilson, J. A., Coalson, T. S., Fischl, B., Andersson, J. L., Xu, J., Jbabdi, S., Webster, M., Polimeni, J. R., Essen, D. C. V., and Jenkinson, M., “The minimal preprocessing pipelines for the human connectome project,” *NeuroImage* **80**, 105–124 (oct 2013).
- [26] Glasser, M. F., Coalson, T. S., Robinson, E. C., Hacker, C. D., Harwell, J., Yacoub, E., Ugurbil, K., Andersson, J., Beckmann, C. F., Jenkinson, M., Smith, S. M., and Essen, D. C. V., “A multi-modal parcellation of human cerebral cortex,” *Nature* **536**, 171–178 (jul 2016).
- [27] Lindquist, M. A., Loh, J. M., Atlas, L. Y., and Wager, T. D., “Modeling the hemodynamic response function in fMRI: Efficiency, bias and mis-modeling,” *NeuroImage* **45**, S187–S198 (Mar. 2009).

- [28] Tomasi, D., Caparelli, E., Chang, L., and Ernst, T., “fMRI-acoustic noise alters brain activation during working memory tasks,” *NeuroImage* **27**, 377–386 (Aug. 2005).
- [29] Raichle, M. E., “The brain’s default mode network,” *Annual Review of Neuroscience* **38**, 433–447 (July 2015).
- [30] Gishkori, S. and Mulgrew, B., “Graph signal processing-based imaging for synthetic aperture radar,” *IEEE Geoscience and Remote Sensing Letters* , 1–5 (2019).
- [31] Jablonski, I., “Graph signal processing in applications to sensor networks, smart grids, and smart cities,” *IEEE Sensors Journal* **17**, 7659–7666 (Dec. 2017).
- [32] Cheung, G., Magli, E., Tanaka, Y., and Ng, M. K., “Graph spectral image processing,” *Proceedings of the IEEE* **106**, 907–930 (May 2018).
- [33] Leonardi, N. and Vile, D. V. D., “Tight wavelet frames on multislice graphs,” *IEEE Transactions on Signal Processing* **61**, 3357–3367 (July 2013).
- [34] Hammond, D. K., Vandergheynst, P., and Gribonval, R., “Wavelets on graphs via spectral graph theory,” *Applied and Computational Harmonic Analysis* **30**, 129–150 (Mar. 2011).